PAPER

Check for updates

Enhanced catalytic performance of single-atom Cu on Mo_2C toward CO_2/CO hydrogenation to methanol: a first-principles study†

Anna Vidal-López, [iD][a] Estefanía Díaz López [iD][a] and Aleix Comas-Vives [iD] *[ab]

CO_2 emissions harm the environment due to their pivotal role in fostering climate change and ocean acidification. One way to take advantage of CO_2 is to use it as a precursor to chemical materials to enable energy transition. The CO_2 to methanol conversion from green H_2 is a promising option. The silica-supported Cu/Mo_2CT_x (MXene) catalyst displayed higher activity than the industrial reference system Cu/ZnO/Al_2O_3. To better understand CO_2 hydrogenation in Cu/Mo_2CT_x and related processes under reaction conditions (CO hydrogenation and reverse water gas shift reaction), we performed periodic DFT calculations to evaluate the methanol synthesis reaction mechanism using our previously calibrated theoretical model against experiment characterization. Our results show the crucial role played by the Cu/Mo_2CT_x interface in providing low-energy pathways to facilitate the hydrogenation of CO_2 to methanol, where both the Cu atom and the Mo_2CT_x support participate in the reaction mechanism. The findings showcase the unique pathways provided by this supported single-atom catalyst, allowing the successive heterolytic cleavages of molecular hydrogen (H_2) to form HCOO*, HCOOH*, and H_2COOH* species with co-adsorbed hydrogen in contrast with classical heterogeneous catalysts based on Cu NPs supported on oxides. Thus, CH_3OH is readily formed under reaction conditions. CO also forms *via* the reverse water-gas shift (RWGS) reaction, which can be hydrogenated to methanol. These findings open new avenues to understanding CO_2 and CO hydrogenation by exploiting single-atom catalysts and metal–support interfaces.

1. Introduction

Climate and energy crises are critical challenges we must face to keep life as we know it. CO_2 is pivotal in this problem,[1] being a primary target to mitigate. To that aim, one strategy is to close the carbon cycle by converting CO_2 to methanol. Methanol is a crucial organic feedstock in the chemical industry as it is a precursor of several valuable chemicals like formaldehyde, acetic acid, and methyl-*tert* butyl ether.[2] Moreover, methanol is an excellent transportation and industrial fuel, able to replace gasoline, diesel fuel, and natural gas. Among different approaches to CO_2 conversion, hydrogenation using "green" H_2 from renewable energy sources is an emergent strategy in the so-called methanol economy framework.[3] The methanol economy is partly based on its production by chemical recycling of CO_2 from the gases of fossil fuel-burning power plants as well

as other industrial and natural sources or even atmospheric CO_2. The methanol economy represents a chemical regenerative carbon cycle alternative to natural photosynthesis. Selecting the appropriate catalyst is crucial to driving the use of hydrogen and avoiding competitive reactions such as the reverse water gas shift (RWGS) reaction. Many heterogeneous catalysts, typically Cu-based, have recently been reported for this purpose.[4,5] The reported Cu-based industrial catalyst (Cu–Zn–Al_2O_3), which displays a highly dynamic nature,[6–10] promotes methanol synthesis[11] from a synthesis gas mixture (CO_2/CO/H_2) at elevated pressures P (50 to 100 bar) and temperatures T (200° to 300 °C).

MXenes[12,13] arise as an attractive family of materials with suitable characteristics such as stability and physical and mechanical properties. They have also displayed attractive electronic, optical, plasmonic, and thermoelectric properties[13] or are emerging materials in thermocatalytic applications.[14] These 2D-materials are a family of transition metal carbides, carbonitrides, and nitrides[15] with the general formula of $M_{n+1}X_nT_x$ (where M is an early transition metal, n = 1, 2, 3, X is C and/or N and T is surface –O–, –OH and/or –F groups). MXenes without surface termination groups are oxophilic; thus, they can bind and activate CO_2.[16] Another class of emerging catalysts is

[a] Department of Chemistry, Universitat Autònoma de Barcelona, 08193 Cerdanyola del Vallès, Catalonia, Spain. E-mail: Aleix.Comas@uab.cat
[b] Institute of Materials Chemistry, Technische Universität Wien, 1060 Vienna, Austria. E-mail: aleix.comas@tuwien.ac.at

† Electronic supplementary information (ESI) available. See DOI: https://doi.org/10.1039/d4cy00703d

6904 | *Catal. Sci. Technol.*, 2024, **14**, 6904–6916

This journal is © The Royal Society of Chemistry 2024

single-atom catalysts (SACs).[17] They are based on an isolated metallic atom stabilized by the support or embedded into another metal. They have shown exceptional performance, drastic cost reduction, high activity, selectivity, metal atom utilization, and stability.[18–20] SACs can incorporate a range of metals, heteroatoms, and supports.[17] Several studies have shown that SACs exhibit superior performance in reactions such as hydrogenation,[21] CO oxidation,[22,23] water-gas shift (RWGS),[24] and CO_2 conversion.[25,26] Moreover, the Cu-SAC family has gained interest due to their ability to convert CO_2 into C_{2+} products with high selectivity.[18] Hence, the combination of 2D materials (MXene) and single-site systems (SACs) has allowed the development of a new framework for hydrogenating CO_2.[27–29]

In a recent study, we reported[30] the catalytic activity of a single Cu atom supported on a molybdenum MXene, Mo_2CT_x. The resulting material, Cu/Mo_2CO_x, had a fixed coverage of 0.67 O* ML during the reaction, and the Cu atom's movement revealed two adsorption sites: one on Mo-hollow sites[30] and another in a bridge position between two Mo atoms. The latter, more stable by 17 kJ mol^{-1}, was used as the reference for energy profile construction in this work. Cu/Mo_2CO_x provides an interface with methanol's increased intrinsic formation rate by hydrogenating CO_2. We benchmarked the theoretical model against the experimental characterization. We found out *via* theoretical models that those with a high oxygen surface lead to a stronger CO adsorption and a higher blueshift in the resulting IR stretching CO frequency, having a high cationic character on the Cu atom, in agreement with IR spectroscopical measurements. Moreover, the H_2 adsorption was more stable on the Cu/Mo_2C interface, which aligned with H_2 thermal programmed desorption (TPD) experiments. These results suggested that the $Cu/2D-Mo_2C$ 0.67 O* ML is a catalytic model in agreement with the experimental characterization. The evaluation of the catalytic activity of the Cu/Mo_2CO_x system by joint experimental and computational work suggested that CO_2 hydrogenation occurred *via* the formate species, which was also detected experimentally. Still, the proposed mechanism of CO_2 hydrogenation over Cu/Mo_2CO_x based on theoretical calculations showed that the most energy-demanding step of the pathway corresponded to the formation of dioxymethylene, having an energy barrier of *ca.* 140 kJ mol^{-1}. Hence, since this barrier is rather energy-demanding, the question of whether alternative pathways can catalyze the methanol formation in an even more feasible way remains open.

Further, the involvement of various reactivity sites of the system (Cu atom, Cu–Mo_2C interface, and support) in a reaction mechanism remains an open question. Besides how the MXene–SAC (Cu/Mo_2CO_x–SiO_2, Fig. 1a) catalyzes the CO/CO_2 hydrogenation, it can provide relevant insights into the catalysis of SACs and the role played by the metal support interface toward the CO_2 hydrogenation in contrast to the mechanisms for typical catalytic/industrial systems based on supported copper nanoparticles such as Cu/ZnO–Al_2O_3 (Fig. 1b).[31]

Moreover, recently, attention has been refocused on the hydrogenation of pure CO_2 or CO_2-rich gas feeds containing carbon monoxide (CO).[32–36] CO is present in the reaction
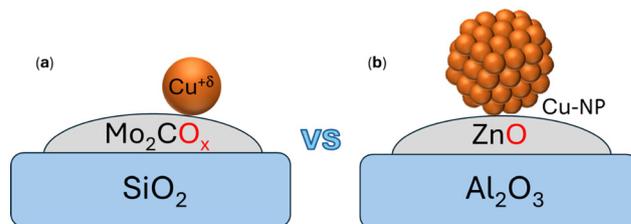

Fig. 1 (a) Representation of the catalytic system (Cu/Mo_2CO_x–SiO_2) used in the study *vs.* (b) the Cu-NP based catalyst (Cu/ZnO_x–Al_2O_3) typically used.

mix, provided that there is activity in the RWGS reaction. Besides, a small fraction of CO_2 in the mixture significantly affects the oxygen chemical potential of the mix.[37–40] One of the most important open questions for Cu-based materials and the Cu/Mo_2CT_x system is the nature of the preferred carbon source to produce methanol: CO or CO_2.[41,42] Also, evaluating the hydrogenation of CO and CO_2 separately is desirable to avoid conflicting views on methanol synthesis, as in the same way as CO_2, CO has many possible reaction pathways our former work did not consider that should be deeply explored. Another critical aspect of direct CO_2 hydrogenation is the competitive RWGS reaction, which decreases the selectivity towards methanol by forming CO, especially in the low-pressure range.[43] The production of large quantities of water may also decrease the catalytic activity and reduce the long-term catalyst stability.[44] Besides, the RWGS reaction is also a highly relevant process.[45–47] In this context, computational chemistry arises as a powerful technique for understanding heterogeneous catalysts[38,48–50] and unraveling the role played by the catalyst at the atomic level in methanol synthesis.[39,40]

For all the noted above, in the present work, we use DFT calculations to answer the critical mechanistic aspects of the CO_2/CO hydrogenation and the RWGS reaction catalyzed by the recently reported Cu/Mo_2CO_x catalyst *via* an extensive mechanistic analysis. The evaluation of the resulting energy profiles provides crucial aspects of the MXene–Cu-based catalyst, such as the role of each catalytic component, the Cu atom, the interface, and the support, besides revealing critical chemical aspects of this material concerning its reactivity and selectivity in the methanol synthesis by CO/CO_2 hydrogenation.

2. Computational details

All DFT calculations were performed using the Vienna *Ab initio* Simulation Package (VASP)[51–53] with a cut-off energy of 500 eV. The structures were optimized using the projector augmented wave (PAW) method (plane-wave basis set with pseudopotentials)[54,55] using the official VASP pseudopotentials[56] and the Bayesian error estimation functional with van der Waals corrections (BEEF-vdW).[57] In the present work context, other research groups have also used it in previous mechanistic studies on CO_2 hydrogenation.

This journal is © The Royal Society of Chemistry 2024

Catal. Sci. Technol., 2024, **14**, 6904–6916 | **6905**

Studt and co-workers compared the performance of the BEEF-vdW with the RPBE functional for the reaction catalyzed by a stepped copper surface,[11] showing that the selectivity with respect to CO and CO_2 in methanol formation is only described correctly with BEEF-vdW in contrast to other commonly used functionals such as RPBE. The electronic SCF-loop (EDIFF) convergence criterion was set to 10^{-5} eV. The convergence criteria for the ionic relaxation were set to forces' norms less than 0.01 eV Å^{-1}. We use the conjugate gradient algorithm (IBRION = 2) to relax the ions. The Monkhorst–Pack with a $3 \times 3 \times 1$ k-point mesh was used to sample the Brillouin zone. The catalyst models were illustrated using Atomic Simulation Environment (ASE), a 3D visualization program for structural models.[58] The energy of isolated molecules was determined by a single-point calculation placing each species in a box with dimensions of $15 \times 15 \times 15$ Å. The nudged elastic band method (NEB)[59] with intermediate images was used to locate all the transition states (TS). Then, all the TS structures were refined using a Newton-based algorithm with the same convergence criteria as for the minima. All reported energy values in the text correspond to electronic energies. In all energy profiles, the values were calculated and referenced against the energy of the initial reactants (in kJ mol^{-1}). Thermodynamic corrections were calculated using statistical thermodynamics at 503.15 K and pressure values of 5 bar (CO_2, H_2O), 15 bar (H_2), and 2.5 bar (CO, CH_3OH) to build the Gibbs energy profile (see the ESI†). The Gibbs energy of the gas phase species was calculated by considering translational, rotational, and vibrational contributions. In contrast, only the vibrational contributions of the chemisorbed species were considered. Finally, an algorithm[60–63] was employed to perform Bader's analysis on a charge density grid, determining the total charge associated with each atom and defining the zero flux surfaces delineating the Bader volumes.

3. Results

3.1 CO_2 and CO hydrogenation and RWGS on the Cu/2D-Mo_2CO_x system

In former work,[30] we evaluated the CO_2 hydrogenation to methanol catalyzed by the Cu/2D-Mo_2C 0.67 O ML surface *via* the BEEF-vdW functional, using a model benchmarked against experimental characterization (Fig. 2a). This work evaluates, using the same model and methodology, how Cu/Mo_2CT_x
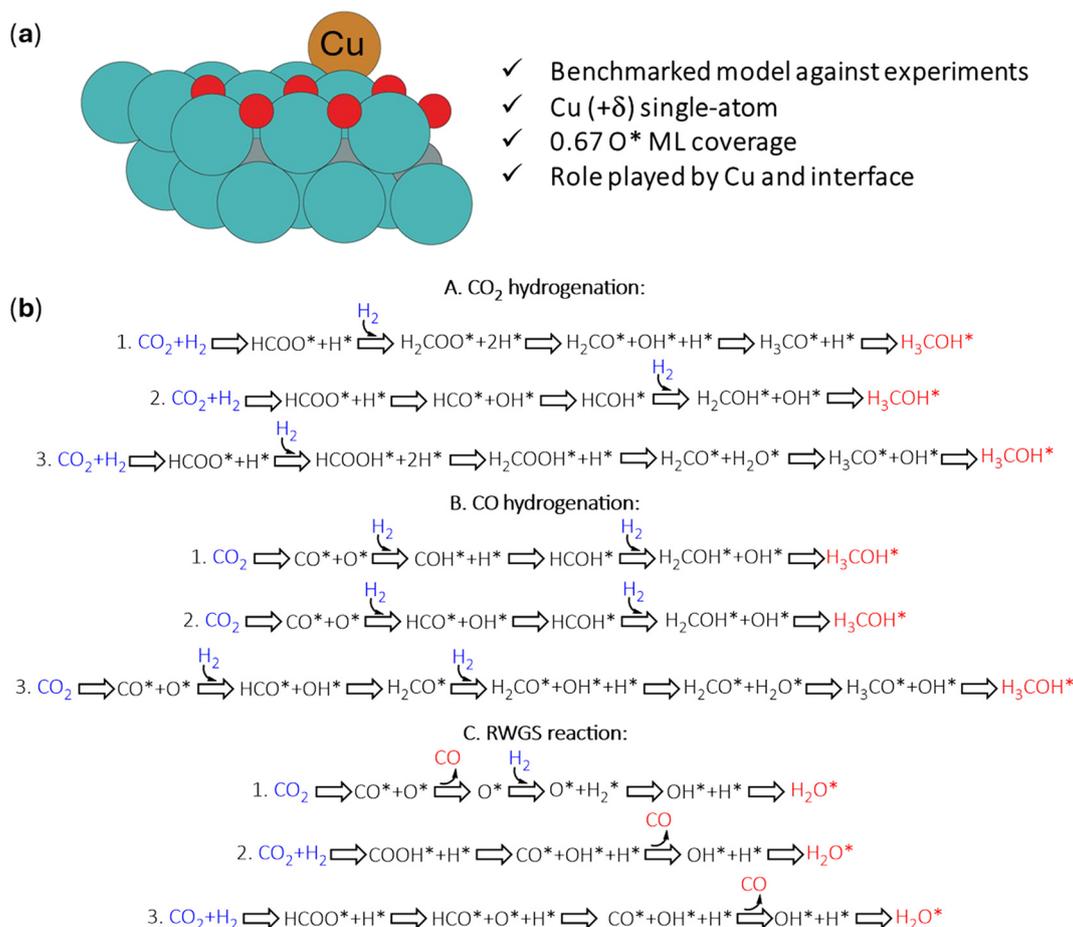

Fig. 2 (a) Optimized structure of the catalytic system (Cu/Mo_2CO_x) used in that study, where the atoms are represented by colors (Cu-ochre, Mo-blue, O-red, H-white, C-gray). (b) Summary of the reactants (blue), intermediates (black), and products (red) involved in each of the different reaction mechanisms reported previously and, in this study, corresponding to the hydrogenation of CO_2 (A) and CO (B) and the competitive RWGS reaction (C).
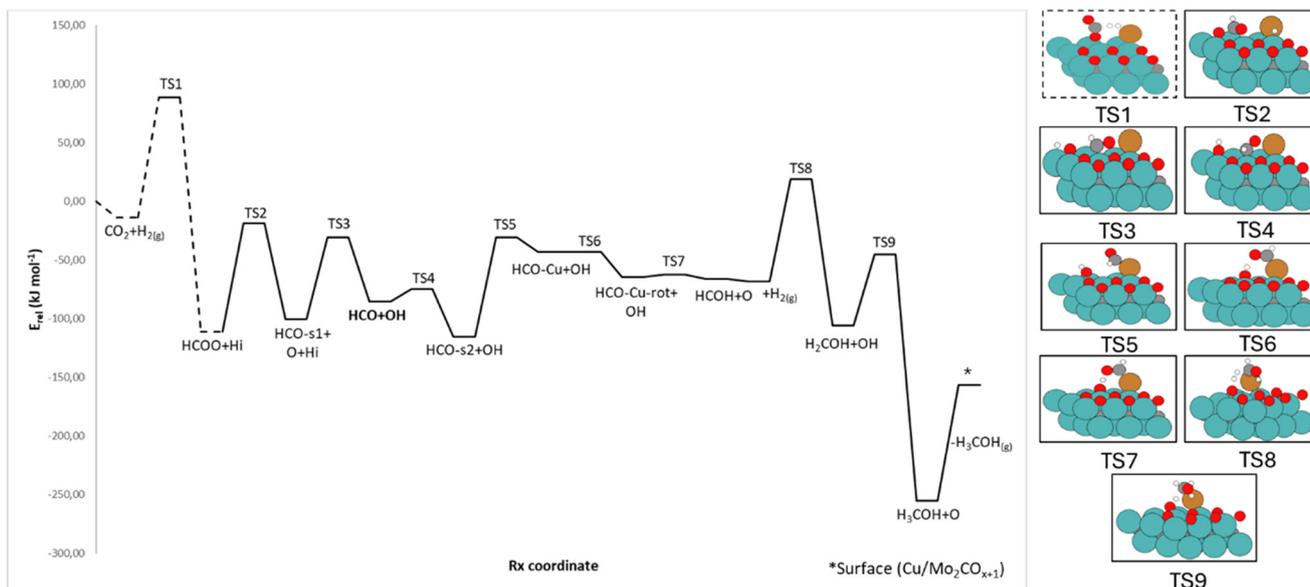
Fig. 3 Energy profile (**A2**) for the reaction of CO_2 and $2H_2$ to form methanol from HCOO* species. Energies of minima and transition states (framed) are referenced against the sum of the initial reactants and catalyst energies in kJ mol^{-1} (E_{rel}).

catalyzes methanol, CO, and water formation from CO_2 and H_2, as summarized in Fig. 2b. We describe each section as the most feasible path based on the calculated energy barriers. By building up on our previous localized intermediates and transition states for this reaction/catalyst (**A1**), we explored additional CO_2 hydrogenation mechanisms (**A2–A3**). Moreover, since Cu/Mo_2CO_x was also found to experimentally form CO under CO_2 hydrogenation reaction conditions *via* the RWGS reaction, we also checked the feasibility of the CO hydrogenation to methanol (**B**), as it is another potential operating route for ultimately catalyzing CO_2 to methanol *via* CO as a reaction intermediate. Moreover, we considered alternative pathways for the competitive reverse water-gas shift (RWGS, **C**) reaction where successive hydrogen transfers to O* to produce water (H_2O*).

3.1.1 CO_2 hydrogenation to methanol. This section discusses the most feasible pathway we located for the methanol synthesis from CO_2 and H_2 (Fig. 2b, **A2**) and the most relevant intermediates and transition states. The first part of the profile corresponds to the hydrogenation of CO_2 to HCOO* (formate). As previously reported,[30] the formation of HCOO* requires an energy barrier of 103 kJ mol^{-1}. The related transition state can be understood as a heterolytic $H_{2(g)}$ cleavage through an Eley–Rideal step since, in the preceding minimum, the hydrogen is in the gas phase, *i.e.*, far from the surface, with an adsorption energy of −0.06 eV and the starting H–H distance of the H_2 molecule (0.739 Å). This transition state forms two new bonds: one H* atom binds to the C atom of CO_2, producing formate (HCOO*), while the other H* atom binds to the Cu/Mo_2CO_x interface. This transition state is analyzed later in detail in the Bader charge analysis section (*vide infra*). Here, we analyze the unreported route (**A2**) shown in Fig. 3 going *via* the **TS2–TS7** transition state structures, which we subsequently describe.

Once HCOO* is obtained, the cleavage of one of the C–O bonds forms HCO* and O* *via* an energy barrier of 92 kJ mol^{-1} (**A2-TS2**). The resulting HCO* is bonded to the Cu center *via* oxygen atoms with an H* (metal hydride) adsorbed at the Cu/Mo_2CO_x interface (HCO-s1) that was produced during the $H_{2(g)}$ heterolytic cleavage. Afterward, OH* forms by combining O* and H*. The formation of the OH* group is required because it participates in subsequent hydrogenation steps, described later. This step must overcome an energy barrier of 70 kJ mol^{-1} (**A2-TS3**). The HCO* species rotation makes the subsequent migration next to the Cu center more feasible. It requires an energy of 11 kJ mol^{-1}, being a shallow and affordable energy barrier (**A2-TS4**). At this point, the HCO-s2* species rotated geometry is obtained. The profile proceeds *via* its migration over the Cu center through a formerly reported transition state (**A2-TS5**), forming the HCO–Cu* species. This step has an energy barrier equal to 85 kJ mol^{-1}. This migration causes a slight rotation of the HCO* compound around the Cu center to facilitate its subsequent hydrogenation (**A2-TS6**) of about 0.3 kJ mol^{-1}, forming the HCO–Cu-rot* species. Afterward, the new configuration promotes the proton transfer from the surface OH* to the HCO* group (**A2-TS7**) subjected to 2 kJ mol^{-1} as an energy barrier, forming O* and HCOH*. Then, the $H_{2(g)}$ molecule splits on O* and HCOH* *via* a heterolytic transition state (**A2-TS8**) as an Eley–Rideal step with an energy barrier equal to 87 kJ mol^{-1}, forming OH* and H_2COH*, respectively. This step is the second most energy-demanding step of this energy profile. The OH* group bonds the Mo_2CO_x surface on the resulting structure, while the H_2COH* species binds the Cu center. Finally, methanol can be readily obtained by proton transfer from the OH* group to H_2COH (**A2-TS9**), with 61 kJ mol^{-1} as an energy barrier. This final state corresponds to the final CH_3OH on the Cu center. Finally, CH_3OH* can be

This journal is © The Royal Society of Chemistry 2024

Catal. Sci. Technol., 2024, **14**, 6904–6916 | **6907**

desorbed, having an energetic cost of 99 kJ mol^{-1}, and water can be easily formed with the oxygen remaining on the surface with two main energy barriers of 73 and 100 kJ mol^{-1} and an endo-energetic desorption by 65 kJ mol^{-1}, as shown in Fig. S1 from the ESI.† Overall, this reaction mechanism provides very feasible energy barriers. The HCOO* formation, the most energy-demanding step of the whole route, has an energy barrier of 103 kJ mol^{-1}. Route **A3** goes through the formation of formic acid (HCOOH*), followed by its hydrogenation (H$_2$COOH*) and its subsequent cleavage to formaldehyde (H$_2$CO). Therefore, these steps present higher energy barriers than the previous **A2** route; thus, this pathway (**A3**) is described in the ESI† (Fig. S2).

The Gibbs energy profile (Fig. S3†) maintains the trend of the electronic profiles. The most notable difference between the two profiles lies in the energy barriers, especially those involving the addition or removal of a gas-phase species, due to the entropic contributions in the energy correction of these species. This occurs when gas-phase incoming molecules react on the surface, such as CO$_2$ or H$_2$, increasing the energy barrier due to the entropic penalty and for the desorption of products, such as CO or methanol and H$_2$O, which are favored entropically.

In summary, we provided more feasible CO$_2$ hydrogenation pathways than the previously reported one.[30] The most feasible mechanism avoids forming dioxymethylene, previously reported as the most energetically demanding step of the CO$_2$ hydrogenation pathway.[30] The most preferred path (**A2**) forms methanol *via* formate (HCOO*), its subsequent cleavage to HCO* and O*, followed by the hydrogenation of HCO* to HCOOH*, H$_2$COH* to form methanol. The evaluated pathways share critical steps and similar energy barriers with the CO hydrogenation mechanism to methanol (*vide infra*).

3.1.2 CO hydrogenation to methanol. This section first presents the methanol formation from CO and H$_2$ using the reaction energies and the resulting energy profiles of the considered pathways (Fig. 2b, **B**). We previously reported[30] that CO* is readily formed by directly activating CO$_2$ adsorbed at the Cu/2D-Mo$_2$C 0.67 O ML interface, yielding CO* and O* species. The first part of the energy profile shows the CO$_2^*$ bending and C–O bond breaking. CO$_2$ pre-activation leads to a structure where the ∠O–C–O angle is *ca.* 136°, and subsequent low energy barriers for the bending and activation equal 35 and 3 kJ mol^{-1}, respectively. Thus, since CO$_{(g)}$ is an experimental product and its formation is highly feasible, the mechanism to hydrogenate CO* to methanol is a route deserving further investigation.

Once CO* is formed, we considered two pathways for its subsequent hydrogenation to methanol: *via* the COH* intermediate or the HCO* one. The formation of COH* species occurs on the Cu atom by hydrogenating the CO* molecule. The COH* pathway (Fig. 2b, **B1**) proceeds *via* subsequent hydrogenations to HCOH*, H$_2$COH*, and methanol species by heterolytic H$_2$ cleavage or transfers of remaining H* at the interface and of protons from OH* groups on the surface. Since already at the thermodynamic

level do the mechanisms and intermediates have a low stability compared to the others (by *ca.* 60–80 kJ mol^{-1}), we did not perform additional transition-state calculations for this pathway.

Conversely, when the HCO* species formation occurs on the support, it is significantly more stable than the COH* one by *ca.* 175 kJ mol^{-1}. Thus, we evaluated three possible mechanisms going through the HCO* intermediate (Fig. 2b, **B2-B2sup-B3**). These mechanisms differ in the reaction intermediates' stabilization energy and the participation of the support in the reaction mechanism. The corresponding three energy profiles, only considering the energetics of the reaction intermediates, are depicted in Fig. S4 in the ESI.† The formed HCO* species is bonded to the Cu center, and one OH* group is also obtained at the Cu/2D-Mo$_2$CO$_x$ surface due to the CO$_2$ cleavage. This process involved the same transition states in the evaluated routes to form the subsequent HCOH and H$_2$CO intermediates.

HCOH path. Fig. 4 presents methanol formation from HCO* species (**B2**) through different intermediates and located transition states (TS), the most favorable pathway among all the evaluated ones. It should be mentioned that the last part of the profile is shared with the route described before for the CO$_2$ hydrogenation described in the former section to generate the HCO* species (**A2**). The first step of this mechanism is the heterolytic cleavage of H$_{2(g)}$ through an Eley–Rideal mechanism that allows obtaining OH* and one H* atom adsorbed on the Cu/Mo$_2$CO$_x$ interface with an energy barrier of 96 kJ mol^{-1} (**B-TS3**). A subsequent transition state to form HCO* by reaction of H* and CO* for HCO* (**B-TS4**) is 102 kJ mol^{-1}. This transition state is the mechanism's most energy-demanding step (RDS). Upon forming the HCO* and OH* species, the mechanism bifurcates into two pathways (**B2, B2-sup**) on the Cu/2D-Mo$_2$CO$_x$ surface. In the first route (**B2**), through the HCOH* species, the reactivity takes place on the Cu center. This pathway exhibits the most feasible energies in terms of transition state energies and reaction energies. Thus, it is described and depicted in Fig. 4. The other path (**B2sup**) on the support is reported in the ESI† (Fig. S5).

Once the HCO* species and the OH* group are obtained, the mechanism forms the HCOH* species through a proton transfer from OH* to HCO*. However, a slight rotation of the HCO* species around the Cu center is first required to enable the subsequent proton transfer. The rotation is about 0.3 kJ mol^{-1} (**B2-TS5**). Afterward, the new configuration allows the proton transfer from the OH* adsorbed on Mo$_2$C to the HCO* group (**B2-TS6**), subjected to 2 kJ mol^{-1} as an energy barrier. Then, when a second H$_{2(g)}$ molecule enters the reactive path, the system slightly stabilizes, releasing 2 kJ mol^{-1}. Subsequently, the H$_{2(g)}$ molecule splits through a heterolytic transition state (**B2-TS7**) as an Eley–Rideal step again with an energy barrier equal to 87 kJ mol^{-1}, forming the H$_2$COH* species coordinated to Cu and an OH* group bonded to the support. This step is the second most energy-demanding for this energy profile. Finally, adsorbed methanol can be readily obtained by proton transfer from the OH* group to H$_2$COH*
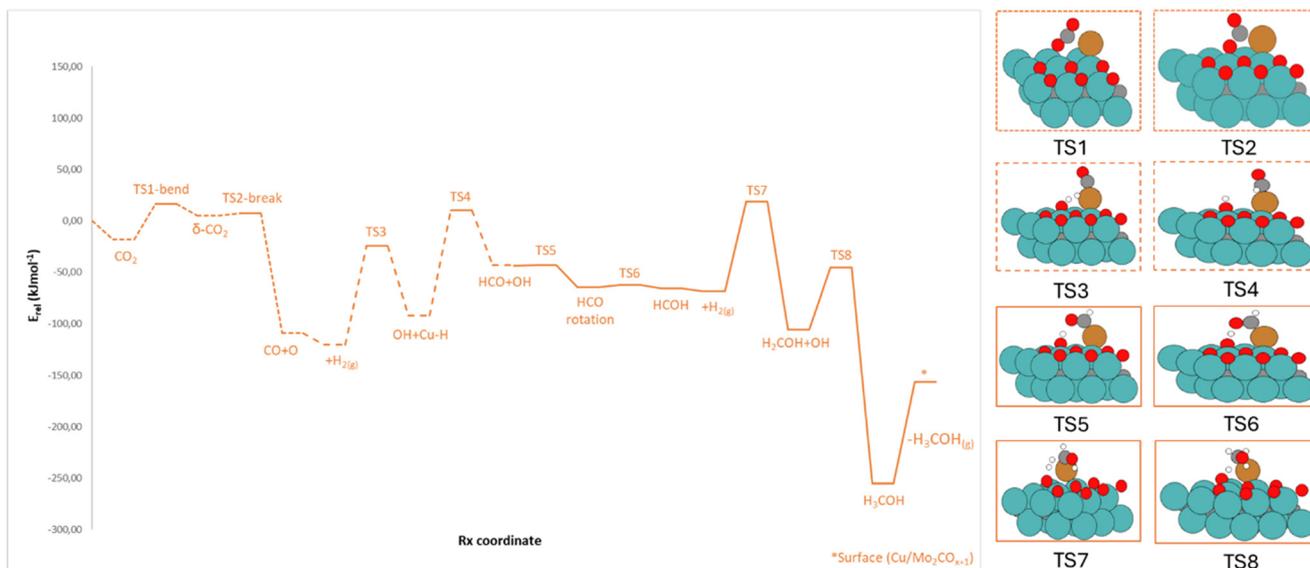
6908 | *Catal. Sci. Technol.*, 2024, **14**, 6904–6916

This journal is © The Royal Society of Chemistry 2024

Fig. 4 Energy profile for the reaction of CO_2 and $2H_2$ to form methanol from the HCOH* species. Dashed traces are steps common for all profiles. Energies of minima and transition states (framed) are referenced against the sum of the initial reactants and catalyst energies in kJ mol^{-1} (E_{rel}).

with 61 kJ mol^{-1} as an energy barrier (**B2-TS8**). Methanol is obtained and adsorbed on the Cu center. Finally, CH_3OH^* can be desorbed as described above on the **A2** profile. The resulting energy profile confirms the feasibility of this reaction mechanism from CO hydrogenation.

Again, the Gibbs energy profile (Fig. S6†) maintains the trend of the electronic energy profile. They showed the same differences described above due to the entropic contributions in the energy correction of these species. Frequency analysis confirmed the nature of all transition states shown in the electron profile, except CO_2 dissociation (**TS2**), where no saddle point was found, *i.e.*, the transition was lower in

Gibbs energy than the respective reactants according to the Gibbs energy. This suggests that the dissociation of CO_2 is practically spontaneous after the formation of bent CO_2, with a CO bond elongated by 1.466 Å.

B2+B2sup path. Fig. 5 presents the last path of this section, namely **B2+B2sup**. This route comprises previous HCOH routes (**B2, B2sup**), connected *via* a transition state (**TS6**). Thus, this pathway goes through the formation of HCO* on the support (Fig. S5†), followed by its hydrogenation to HCOH* on Cu (Fig. 4).

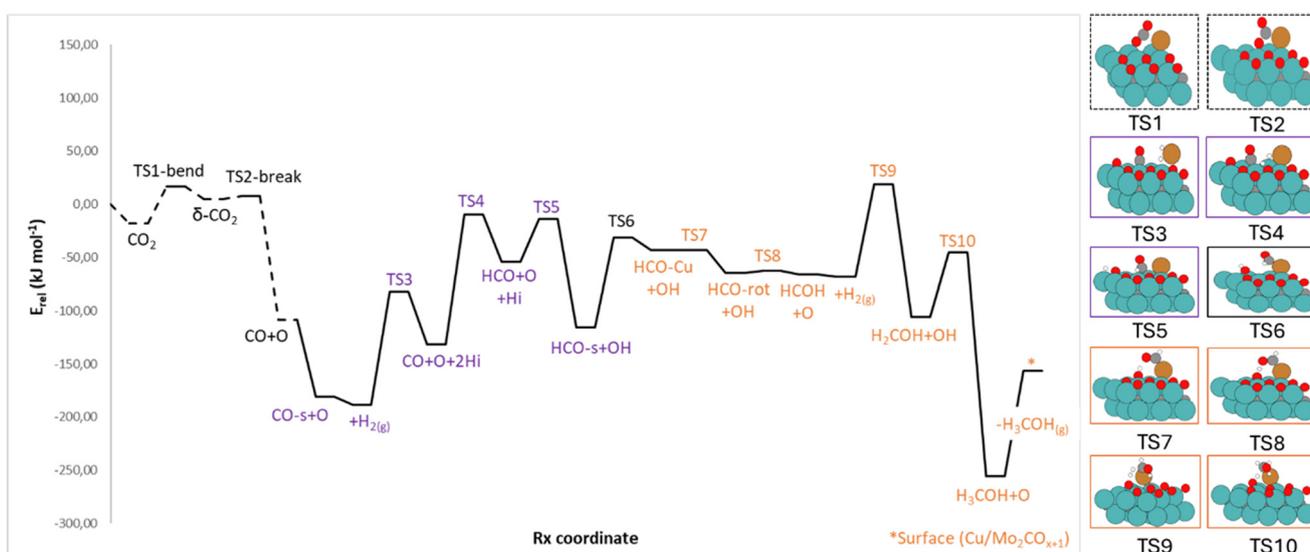This mechanism starts with the CO* migration from Cu to the Mo₂C support, where its stabilization increases

Fig. 5 Energy profile for the reaction of CO_2 and $2H_2$ to form methanol from HCOH* species on the support (purple labels) to HCOH* species on the Cu center (orange labels). The dashed line shows steps that are common for all profiles. Energies of minima and transition states (framed) are referenced against the sum of the initial reactants and catalyst energies in kJ mol^{-1} (E_{rel}).

considerably, releasing 72 kJ mol^{-1}. In this case, the C atom of CO* is directly bonded to Mo hollow sites, and its desorption has an energy cost of 152 kJ mol^{-1}, much higher than the CO desorption energy from the Cu atom. After that, a new molecule of H$_{2(g)}$ participates in the pathway. In contrast to the previously evaluated paths, its activation proceeds *via* a homolytic transition state (**B2sup-TS3**) *via* an Eley–Rideal step, having an energy barrier of 107 kJ mol^{-1} and forming a couple of H–Cu bonds. The preference for the homolytic cleavage of H$_2$ is probably due to the distance between the CO* group and the Cu interface (3.165 Å), which does not allow a heterolytic cleavage. Once this activation occurs, the mechanism forms HCO* species by transferring the H* from the Cu/Mo$_2$CO$_x$ interface to CO*, with an energy barrier of 122 kJ mol^{-1} (**B2sup-TS4**). Afterward, we considered the OH* formation by hydrogen transfer from the second H*, having an energy barrier of 40 kJ mol^{-1} (**B2sup-TS5**). Thus, the step sequence ends when both HCO* and co-adsorbed OH* species are obtained at the Mo-hollow sites of the support. Overall, this route allows the formation of the HCO* intermediate *via* one of the lowest energy barriers obtained. The next step (**TS6**) connects the HCOH-support pathway (**B2-sup**) with the HCOH one (**B2**). This transition state corresponds to the simultaneous migration of the HCO* species to Cu and OH* near the Cu/Mo$_2$CO$_x$ interface. This step requires an energy barrier of 85 kJ mol^{-1}. Therefore, at this point, the subsequent reactions leading to methanol directly involve the Cu center (orange labels), as described in the main text in the HCOH-path section (Fig. 3, **B2**). This mixed route is possibly another feasible mechanism for obtaining methanol despite the higher values of some energy barriers, namely 107 and 122 kJ mol^{-1} for the hydrogen activation and HCO formation steps, respectively. The final Gibbs energy profile (Fig. S7†) was also analyzed, maintaining the trends of the electronic energy profile.

The other energy profiles *via* the HCO* species are described in the ESI† due to their higher energy barriers. The first one (**B2sup**) considers the formation and hydrogenations of HCO* on the support because it considers the prior migration of CO* from the Cu atom to the 2D-Mo$_2$CO$_x$ support, increasing its stability (Fig. S5†). The second one forms formaldehyde (**B3**, H$_2$CO*), where the chemistry moves from the Cu atom to the support and its subsequent hydrogenations to methoxy and methanol species (Fig. S8†).

In summary, DFT calculations suggest a feasible energy profile for the CO hydrogenation pathway to methanol catalyzed by the Cu/2D-Mo$_2$C 0.67 O ML system. This occurs *via* the HCOH intermediate on the Cu atom through the HCO species (**B2** pathway). The Cu atom, the Cu/Mo$_2$CO$_x$ interface, and the support provide active sites and play a crucial role in the CO hydrogenation reaction. Among all the profiles, we can see their active participation in the reaction mechanism by simultaneously lowering the energy barriers for successive heterolytic H$_{2(g)}$ cleavages required to form HCO*, HCOH*, and H$_2$COH* species, respectively, besides H* adsorbed at the interface. The most energetically

demanding step of the most affordable energy path leading to methanol is the formation of the HCO* species (102 kJ mol^{-1}) with an energy barrier like the reported one[30] for HCOO* formation.

Competition and selectivity. After the electronic and Gibbs energies for the evaluated pathways have been obtained, it is necessary to discuss their competition and how it may affect the selectivity toward CO or CH$_3$OH. We need to consider the energy values comprising barriers and desorption.

Concerning CO$_2$, the most plausible route to obtain methanol (**A2** path) is through the HCO* species obtained by the previous dissociation of HCOO*. The energy barrier associated with the formation of HCOO* is about 103 kJ mol^{-1}, and its dissociation to HCO* and O* of 92 kJ mol^{-1}. The HCO* is subsequently hydrogenated to methanol or can be dissociated into CO* and H* with an energy barrier of 100 kJ mol^{-1}, suggesting CO* as a feasible side product of the pathway.

Concerning CO as a reactant, it has three significant barriers that might affect the selectivity of the reaction. CO* formation is less energy-demanding than the HCOO* one since its cleavage into CO* and O* is *ca.* 35 kJ mol^{-1}. Its subsequent hydrogenation to HCO* (**B2** path) is a two-step process involving energy barriers of 96 kJ mol^{-1} and 102 kJ mol^{-1} for the H$_{2(g)}$ heterolytic activation and the subsequent HCO* formation, respectively. On the other hand, the CO desorption costs 80 kJ mol^{-1}. CO can also migrate from the Cu atom to the support, *i.e.*, towards a hollow-Mo site of Mo$_2$C (**B2sup**). This step is favorable by 72 kJ mol^{-1} upon adsorption. Thus, the CO* desorption from the support has an energy cost of 152 kJ mol^{-1}, much higher than the CO desorption energy from the Cu atom. Hence, this route will likely increase selectivity toward methanol since CO desorption is difficult. At the same time, the hydrogenation of CO* (CO-s) is more feasible energetically, *i.e.*, the formation of the HCO* species is the highest energy barrier toward methanol, with an energy barrier of 122 kJ mol^{-1}. These results suggest the preference for CO-s to be hydrogenated rather than desorbed.

Evaluating the Gibbs profiles and the computed energies about barriers, we observed the same tendency as in the electronic scenario described above, considering the thermodynamic corrections. The critical difference in Gibbs energies compared to the electronic energies is that CO desorption becomes easier than the respective transition state of hydrogenation, both from Cu and the support (by 107 kJ mol^{-1} and by 48 kJ mol^{-1}, respectively). Nevertheless, since the gas-phase CO and CH$_3$OH have similar energy (CO is more stable in Gibbs energy than methanol by only 16 kJ mol^{-1}) and the Gibbs energy barriers for hydrogenation are affordable under the evaluated conditions, one can expect forming both products, without having a high selectivity for either of them.

3.1.3 RWGS on the Cu/2D-Mo$_2$CO$_x$ surface. The last section shows the results of the competitive reverse water-gas shift reaction (RWGS, Fig. 2, **C**). As reported in our previous work,[30]
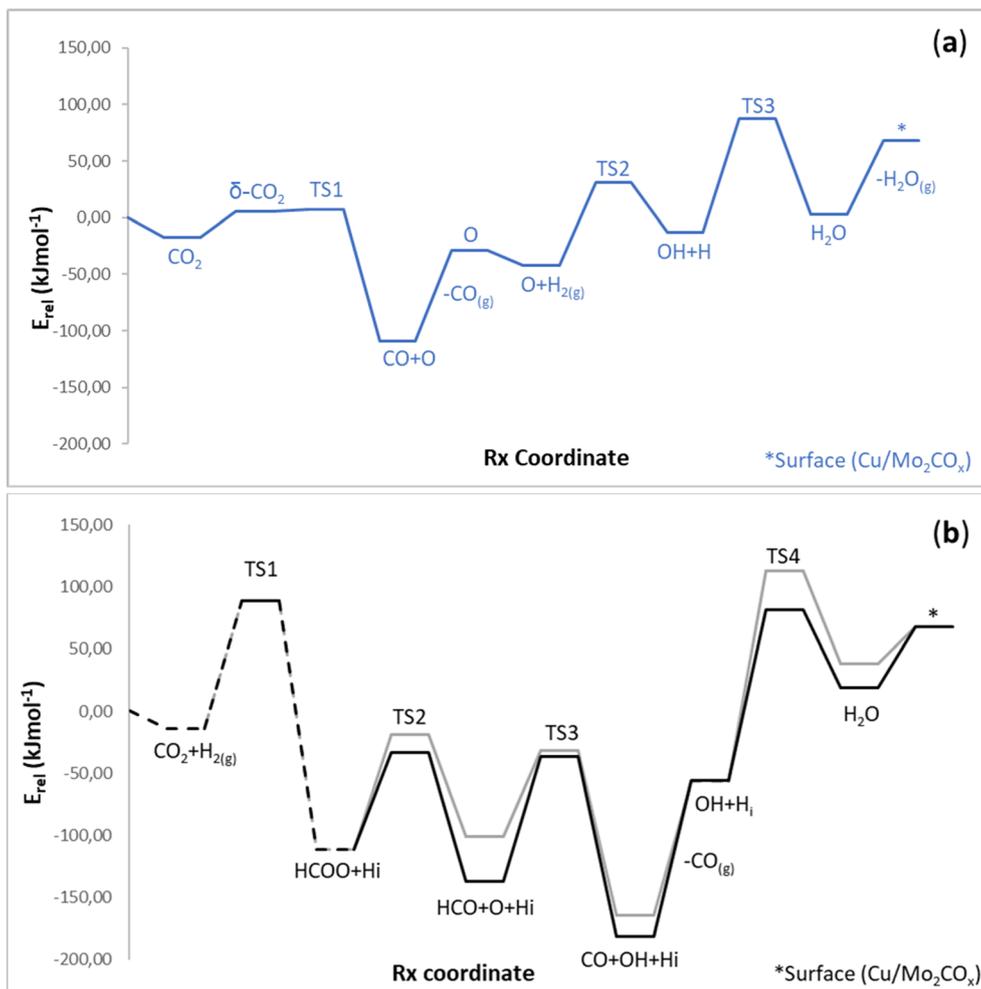
6910 | *Catal. Sci. Technol.*, 2024, **14**, 6904–6916

This journal is © The Royal Society of Chemistry 2024

Fig. 6 Energy profiles for the RWGS reaction of CO and H_2 to form water through two different pathways: (a) CO* + O* (blue line) or (b) HCOO* (**C21**-gray and **C22**-black lines), respectively. Intermediates in the dashed line are common in more than evaluated pathways. Energies are referenced against the initial reactants' energy in kJ mol^{-1} (E_{rel}).

CO_2 can be pre-activated at the Cu/2D-Mo_2C 0.67 O ML *via* its easy chemisorption, in which the δ-CO_2 species bends. Subsequently, this bent species can either directly cleave one C–O bond or hydrogenate by transferring a co-adsorbed H* species. This section presents the evaluated possible pathways to form CO* and water from CO_2 and H_2 through probable intermediates *via* COOH* (**C2**) and HCOO* (**C3**) species. The description and the representation of each path based on the energies of the intermediates, *i.e.*, thermodynamics, are included in the ESI† (Fig. S9).

All pathways start with the bending of CO_2, which is pre-activated *via* its bending (∠O–C–O is *ca.* 136°), having an energetic cost of 35 kJ mol^{-1}. Then, the mechanism (Fig. 2, **C1**) can proceed through the C–O cleavage with the lowest energy barrier, about 3 kJ mol^{-1}. Thus, after CO desorption, which required 80 kJ mol^{-1}, $H_{2(g)}$ was energetically favorably adsorbed on the Cu atom by 13 kJ mol^{-1}. H_2^* was coordinated to the Cu atom in a η² mode with an H–H distance of 0.759 Å and −0.44 eV as adsorption energy. Thus, in the next step, through a Langmuir–Hinshelwood path, the heterolytic cleavage of H_2^*

simultaneously produced O–H and Cu–H bonds. This step was endo-energetic by 29 kJ mol^{-1} with an energy barrier of 73 kJ mol^{-1}. Finally, H_2O^* was formed by the subsequent reaction of OH* with H* at the interface, with an energy barrier of 100 kJ mol^{-1}, *i.e.*, the rate-limiting step of the RWGS pathway. The resulting intermediate was 3 kJ mol^{-1} higher than the initial reactants. The final step, *i.e.*, water desorption, was endo-energetic and required 65 kJ mol^{-1} (see below, Fig. 6a).

Next, we describe the most feasible pathways from the δ-CO_2 species forming the HCOO* species (**C3**). Here, we discuss the transition states of the most viable routes, taking those with the most stable reaction intermediates. It is written with more details in the ESI, where the corresponding energies of each intermediate and transition state are also provided. The COOH* species (**C2**) formation from the δ-CO_2 and subsequent water formation are described in the ESI† (Fig. S10).

HCOO routes. The HCOO route begins with the direct hydrogenation of CO_2 to obtain HCOO* on the support. This heterolytic transition state (**A2-TS1**) formally produces a

This journal is © The Royal Society of Chemistry 2024

Catal. Sci. Technol., 2024, **14**, 6904–6916 | **6911**

metal hydride and a positive H* attached to a carbon atom from the bent CO_2^*. This step required an energy barrier of 103 kJ mol^{-1} (**TS1**, Fig. 3). As mentioned above, the HCOO* intermediate on RWGS can take different pathways to obtain water from HCOO* cleavage. We subsequently describe the two most feasible energy routes (Fig. 6b): **C3-1** (gray) and **C3-2** (black).

The **C3-1** route from HCOO* starts with its cleavage into HCO* and O* species in the Mo-hollow site with an energy barrier of 92 kJ mol^{-1} (**C3-1 TS2**). In this step, the C–O cleavage occurs on the oxygen far from the copper atom. The HCO* and H* atoms are then adsorbed at the Cu/2D-Mo$_2$C 0.67 O ML interface. After that, HCO* promotes proton transfer to obtain the OH* group via an energy barrier of 69 kJ mol^{-1} (**C3-1 TS3**). Thus, in this third transition state, CO* forms on the Cu atom while the OH* group remains on the surface and the H* atom on the interface. The CO* can then be desorbed in a step endo-energetic by 109 kJ mol^{-1}. The final step for water formation is the transfer of the proton at the interface to the OH* with an energy barrier of 170 kJ mol^{-1} (**C3-1 TS4**), the most energy-demanding step of the mechanism. Finally, water can be desorbed by 30 kJ mol^{-1}. The ESI† (Fig. S11) shows the resulting energy profile.

The **C3-2** route from HCOO* started with its cleavage into HCO* and O* species in Mo-hollow with an energy barrier of 77 kJ mol^{-1} (**C3-2 TS2**). The C–O bond split through the oxygen next to the copper atom. HCO* is adsorbed in Mo-hollow, while H* is at the metal–surface interface. After that, HCO* promotes the transfer of the proton to the adsorbed oxygen atom (O*) through an energy barrier of 100 kJ mol^{-1} (**C3-2 TS3**). In this transition state, the CO* and OH* groups remain on the surface at the Mo-hollow sites. The CO* can then be desorbed at an energy cost of ca. 125 kJ mol^{-1} due to its higher stability when adsorbed on the support compared to when adsorbed on the Cu center (CO + OH + H$_i$: Fig. S11,† −164 kJ mol^{-1} vs. Fig. S12,† −181 kJ mol^{-1}). The final step for water formation is the transfer of the proton from the H* atom at the interface to OH* with an energy barrier of 138 kJ mol^{-1} (**C3-2 TS4**). Again, obtaining H$_2$O* is the most energy-demanding step of this second mechanism on the HCOO* intermediate. Finally, water desorption costs 49 kJ mol^{-1}. The ESI† (Fig. S12) shows the resulting energy profile.

At this point, it is necessary to compare the new RWGS pathways, forming CO and H$_2$O via the HCOO* intermediate with the previous results[30] of the direct CO$_2$ activation to CO* and O*, CO desorption, and the water formation from O* (described above). Fig. 6a and b show the energy profiles corresponding to the cleavage of the formate (gray, black) with the first step (**TS1**) in common (dashed) and from the activation of CO$_2$ (blue). The first difference between the two reaction mechanisms (HCOO vs. CO) is the first transition state. Formate formation shows a higher energy barrier than for cleavage of the previously activated C–O bond, ca. 102 kJ mol^{-1}, as described in the previous profiles in this manuscript. From here, the hydrogenation of the oxygen cleaved from CO$_2$ presents two more TS with energy barriers

of 73 and 100 kJ mol^{-1}, respectively, already reported.[30] In the case of TS on the HCOO route, the following are mentioned: it must be said that the barrier to obtaining formate is feasible, being a species detected experimentally.[30] Therefore, in this case, the formation of H$_2$O marks the viability of one or another mechanism. In this case, the CO$_2$ cleavage pathway (blue) is the one with the lowest barrier, approximately 38 kJ mol^{-1} compared to HCOO (Fig. 6, a-blue line: **TS3** – 100 kJ mol^{-1} vs. b-black line: **C3-2 TS4** – 138 kJ mol^{-1}).

In summary, the DFT calculations allowed studying alternative pathways for obtaining water in the RWGS compared to the previous route explored through CO* and O* species on the Cu/2D-Mo$_2$C 0.67 O ML model.[30] Also, they highlight the possible intermediates and transition states. The copper atom, the support, and the interface between them participate in the reaction mechanism by reducing the energy barriers heterolytic cleavages of H$_2$ required to form HCOO* and COOH* species, simultaneously with H* adsorbed or cleaved bonds. The most energy-demanding step of the COOH pathway is the formation of CO* and OH* species (**C2-TS2**, 139 kJ mol^{-1} in Fig. S10†). In contrast, for HCOO pathways, the most energy-demanding step is forming water (**C3-1 TS4**, 170 kJ mol^{-1} in Fig. S11† and **C3-2 TS4**, 138 kJ mol^{-1}, in Fig. S12†). Based on the energy barriers, the formation of the HCOO* intermediate is more likely than the COOH* one. Moreover, the water formation step determines the preferred RWGS mechanism, corresponding to the direct cleavage of CO$_2$ to CO* and O*, followed by CO* desorption and the subsequent hydrogenation of O* to form H$_2$O.

3.2 Bader charge analysis

The nature of the observed heterolytic cleavage was of interest to understanding the mechanism of successive hydrogenations. In contrast, the activation of CO$_2$ and H$_2$ was also analyzed. We used the Bader charge analysis for this approach.[60–63] This computational tool allows us to obtain valuable information about the charge change along the evaluated reaction paths, highlighting the importance of the Cu/Mo$_2$CO$_x$ interface in the reaction mechanism.

According to the previous results (see Fig. 3 and 4), we found several steps for which the direct cleavage for the H$_{2(g)}$ molecule showed charge polarization between the hydrogen atoms on the transition states, suggesting the heterolytic cleavage of H$_{2(g)}$. This scenario is present for structures along all the reaction profiles for CO$_2$ hydrogenation (a), CO hydrogenation (b), and RWGS (c). This cleavage also allowed the production of formate and hydroxymethylene (HCOH) hydrogenation on the CO$_2$ hydrogenation profile before obtaining methanol. On the CO hydrogenation, a similar H$_{2(g)}$ heterolytic cleavage is found for the previous step of HCO formation and the HCOH hydrogenation, as mentioned before. On the RWGS, this transition state was observed before the water formation step through an adsorbed H$_2^*$, as reported in previous studies.[30]

6912 | Catal. Sci. Technol., 2024, **14**, 6904–6916

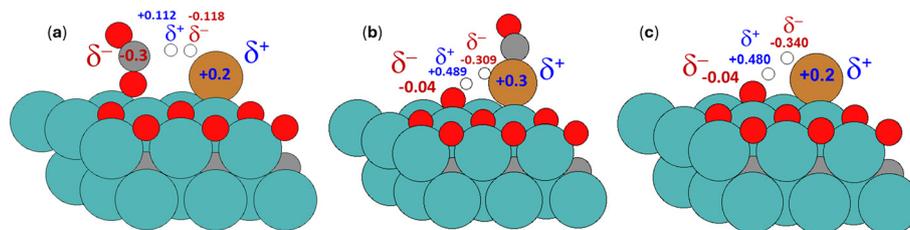This journal is © The Royal Society of Chemistry 2024

Fig. 7 Bader charges aquired by the key atoms involved in the transition states (positive in blue, negative in red) corresponding to HCOO formation on CO_2 hydrogenation (a), in CO hydrogenation (b), and the key step in the water formation path (c).

Bader charge analysis shows a negative charge (red) acquired by the carbon or oxygen atom as they hydrogenate. In contrast, the Cu atom had a positive charge value (blue) due to hydride formation, as depicted in Fig. 7. The results suggest a heterolytic cleavage of $H_{2(g)}$, as reported in the abovementioned energy barriers. This type of cleavage is associated with relatively energy-demanding energy barriers (kJ mol^{-1}) because it involves two different bonding processes of breaking and forming in a single-step transition state. However, the reported energy barriers are affordable, in a range of 73–102 kJ mol^{-1} in different scenarios (Fig. 7) and provide unique paths characteristic of single-atom catalysts, differing from those on extended Cu metal surfaces, present on Cu NPs supported on oxides.

On the other hand, we also analyzed the Bader charges for the CO_2 activation to CO* and O*. Fig. 8a shows the trend along the CO_2 activation path to CO* and O*. The first transition state presented the bending from its linear equilibrium geometry for the uncharged state, which required a slight energy barrier. This bending (180 to 157°) induces changes in the shape and energy level of the molecular orbitals, possibly stabilizing the LUMO on the carbon and making it more electrophilic, as suggested in the literature.[64] Bader values on the TS and δ-CO_2 indicated the negative character added (+0.19) on the carbon and oxygen atoms by increased reactivity due to the bending step. The C

atom bonded with Cu on the interface while remaining bonded to the oxygen atoms. The bond length is elongated on the resulting bent configuration, indicating the weakening of the C–O bond. The second transition state shows CO_2 polarization between the C–O group and oxygen near Mo sites. Then, it takes the formation of two new bonds: OC–Cu and O–Mo. This cleavage is favored by the electron-transfer process between C (negative character) and O (positive character), which is facilitated when CO_2 is bent as the LUMO level lowers its energy.[64] Next, Bader values indicated carbon monoxide formation where C localized negative charge due to being bonded to O and Cu while these last two atoms remain positive. Finally, the activation of the H_2 molecule was also evaluated along the CO hydrogenation pathway (Fig. 8b). Conversely to the former cases, this activation goes through a homolytic cleavage on the Cu atom, which has an energy barrier of 106 kJ mol^{-1}. The Bader charge analysis showed that both H atoms acquire a negative charge when bonded to the Cu atom. Thus, there was no difference in charge polarization between the hydrogen atoms for this cleavage, while Cu also acquired a positive charge (Fig. 8c).

Thus, *via* Bader charge analysis, we further characterize the nature of the bond cleavages along the critical reaction intermediates along the methanol path. *Via* this analysis, we can also confirm the crucial role of the interface and the Cu
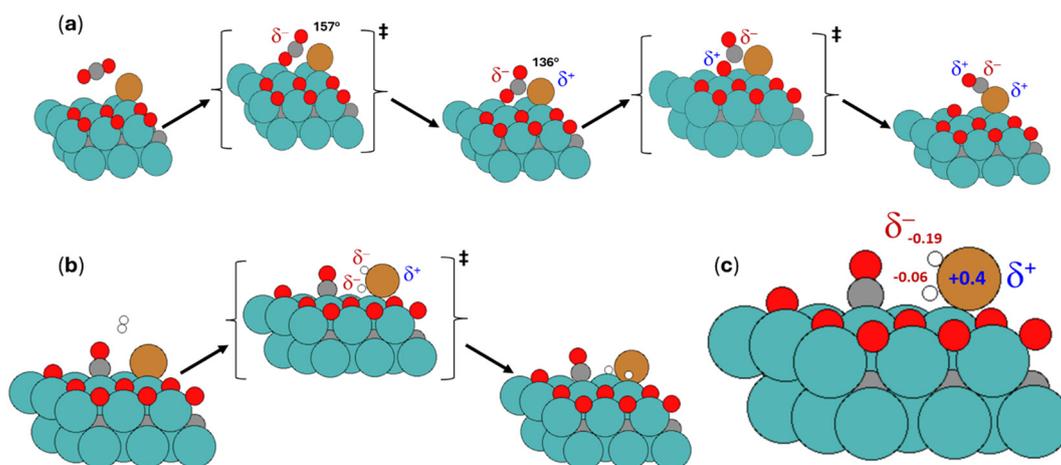

Fig. 8 (a) Optimized geometries of minima and transition states obtained for the CO_2 activation into CO* and O*. It also depicts the degree of bending of CO_2 and the character acquired by the atoms involved. (b) Optimized geometries of minima and transition states were obtained for the H_2 activation. (c) Bader charges aquired by the key atoms involved in the transition states (positive in blue, negative in red).

atom in driving methanol synthesis, where the latter actively participates in the cleavages; the interface allows the resulting species to be firmly bonded to the system, avoiding their desorption. All the calculated Bader values in this section are summarized in the ESI† (Tables S13–S15).

4. Conclusions

We evaluated *via* first-principles calculations the mechanism of methanol and water formation from CO_2/CO and H_2 catalyzed by the Cu/2D-Mo_2C 0.67 O ML model, finding additional feasible routes for CO_2 hydrogenation to those previously reported.[30] The energy barriers confirm that the route *via* HCOO*, HCO*, HCOH*, and H_2COH* as reaction intermediates allows methanol production *via* lower energy barriers than those previously reported (**A2** path). Formate formation is the most energy-demanding step for these alternative pathways. On the other hand, the best and easiest way to obtain CO is by directly cleaving CO_2, forming CO* and O*. Subsequently, the most feasible path for the CO hydrogenation to methanol occurs *via* the HCOH* intermediate (**B2** path) from HCO* species adsorbed on Cu. Also, the migration of CO to the support and its subsequent hydrogenation, as described on the **B2+B2sup** path, is another feasible mechanism for obtaining methanol. Based on the electronic and free energies evaluated, we can conclude that CH_3OH and CO formation are affordable under reaction conditions. Therefore, the catalytic system allows both, and it seems reasonable that there is no high selectivity toward either of the two products.

Our study revealed that the Cu/Mo_2CO_x interface is crucial in providing low-energy pathways for CO_2/CO hydrogenation to methanol. Both the Cu atom and the Mo_2CO_x support are actively involved in the reaction mechanism, facilitating successive heterolytic cleavages of molecular hydrogen (H_2) to form critical intermediates such as HCOO*, HCOOH*, H_2-COOH*, and H_3CO*. This contrasts with classical heterogeneous catalysts based on Cu nanoparticles supported on oxides. We found that the most energy-demanding step in these pathways is the formation of HCOO* or HCO* species, with energy barriers around 103–102 kJ mol^{-1}, respectively. Our results also identified feasible energy profiles for the RWGS reaction, with the HCOO* pathways (**C3** path) more likely than *via* the COOH* species (**C2**). DFT calculations highlight the most likely intermediates and transition states and allow us to propose a feasible energy profile on the Cu/2D-Mo_2C 0.67 O ML. The most energy-demanding step of the HCOO pathways is forming water. Nevertheless, the most viable paths to obtain CO* and H_2O* are those starting with the direct cleavage of one C–O bond of CO_2.

Using Bader charge analysis, we confirmed the nature of the heterolytic cleavages that enable successive hydrogenations, highlighting the crucial role of charge polarization. These findings provide insights into CO_2 and CO hydrogenation, demonstrating the unique advantages of single-atom catalysts and metal–support interfaces in enhancing catalytic performance.

Data availability

Data for this article, including input and output files will be available at Zenodo at [https://doi.org/10.5281/zenodo.13950412].

Conflicts of interest

There are no conflicts of interest to declare.

Acknowledgements

References

1 S. Solomon, G.-K. Plattner, R. Knutti and P. Friedlingstein, Irreversible climate change due to carbon dioxide emissions, *Proc. Natl. Acad. Sci. U. S. A.*, 2009, **106**(6), 1704–1709.

2 A. Goeppert, M. Czaun, J.-P. Jones, G. K. Surya Prakash and G. A. Olah, Recycling of carbon dioxide to methanol and derived products—closing the loop, *Chem. Soc. Rev.*, 2014, **43**(23), 7995–8048.

3 G. A. Olah, Beyond oil and gas: the methanol economy, *Angew. Chem., Int. Ed.*, 2005, **44**(18), 2636–2639.

4 R. Guil-López, N. Mota, J. Llorente, E. Millán, B. Pawelec, J. L. G. Fierro and R. M. Navarro, Methanol Synthesis from CO_2: A Review of the Latest Developments in Heterogeneous Catalysis, *Materials*, 2019, **12**(23), 3902–3926.

5 S. T. Yong, C. W. Ooi, S. P. Chai and X. S. Wu, Review of methanol reforming-Cu-based catalysts, surface reaction mechanisms, and reaction schemes, *Int. J. Hydrogen Energy*, 2013, **38**(22), 9541–9552.

6 M. Behrens, F. Studt, I. Kasatkin, S. Kühl, M. Hävecker and F. Abild-Pedersen, *et al.*, The active site of methanol synthesis over Cu/ZnO/Al_2O_3 industrial catalysts, *Science*, 2012, **336**(6083), 893–897.

7 T. Lunkenbein, J. Schumann, M. Behrens, R. Schlögl and M. G. Willinger, Formation of a ZnO overlayer in industrial Cu/ZnO/Al_2O_3 catalysts induced by strong metal-support interactions, *Angew. Chem., Int. Ed.*, 2015, **54**(15), 4544–4548.

8 R. Schlögl, Chemical batteries with CO_2, *Angew. Chem., Int. Ed.*, 2022, **61**(7), e202007397.

9 G. Pacchioni, From CO_2 to Methanol on Cu/ZnO/Al_2O_3 Industrial Catalyst. What Do We Know about the Active Phase and the Reaction Mechanism?, *ACS Catal.*, 2024, **14**(4), 2730–2745.

10 A. Beck, M. A. Newton, L. G. van de Water and J. A. van Bokhoven, The Enigma of Methanol Synthesis by Cu/ZnO/Al_2O_3-Based Catalysts, *Chem. Rev.*, 2024, **124**(8), 4543–4678.

11 F. Studt, F. Abild-Pedersen and J. B. Varley, *et al.*, CO and CO_2 Hydrogenation to Methanol Calculated Using the BEEF-vdW Functional, *Catal. Lett.*, 2013, **143**, 71–73.

12 S. Posada-Pérez, P. J. Ramírez, R. A. Gutiérrez, D. J. Stacchiola, F. Viñes and P. Liu, *et al.*, The conversion of CO_2 to methanol

6914 | *Catal. Sci. Technol.*, 2024, **14**, 6904–6916

This journal is © The Royal Society of Chemistry 2024

on orthorhombic β-Mo$_2$C and Cu/β-Mo$_2$C catalysts: mechanism for admetal induced change in the selectivity and activity, *Catal. Sci. Technol.*, 2016, **6**, 6766–6777.

13 B. Anasori, M. R. Lukatskaya and Y. Gogotsi, 2D metal carbides and nitrides (MXenes) for energy storage, *Nat. Rev. Mater.*, 2017, **2**, 16098.

14 A. Kurlov, E. B. Deeva and P. M. Abdala, *et al.*, Exploiting two-dimensional morphology of molybdenum oxycarbide to enable efficient catalytic dry reforming of methane, *Nat. Commun.*, 2020, **11**, 4920.

15 M. Naguib, M. Kurtoglu, V. Presser, J. Lu, J. Niu and M. Heon, *et al.*, Two-dimensional nanocrystals produced by exfoliation of Ti$_3$AlC$_2$, *Adv. Mater.*, 2011, **23**(37), 4248–4253.

16 Á. Morales-García, A. Fernández-Fernández, F. Viñes and F. Illas, CO$_2$ abatement using two-dimensional MXene carbides, *J. Mater. Chem. A*, 2018, **6**, 3381–3385.

17 C. E. Creissen and M. Fontecave, Keeping sight of copper in single-atom catalysts for electrochemical carbon dioxide reduction, *Nat. Commun.*, 2022, **13**, 2280.

18 N. Cheng, L. Zhang and K. Doyle-Davis, *et al.*, Single-Atom Catalysts: From Design to Application, *Electrochem. Energy Rev.*, 2019, **2**, 539–573.

19 H. Wei, X. Liu and A. Wang, *et al.*, FeOx-supported platinum single-atom and pseudo-single-atom catalysts for chemoselective hydrogenation of functionalized nitroarenes, *Nat. Commun.*, 2014, **5**(1), 1–8.

20 B. Qiao, A. Wang and X. Yang, *et al.*, Single-atom catalysis of CO oxidation using Pt$_1$/FeOx, *Nat. Chem.*, 2011, **3**(8), 634–641.

21 Y. Lu, J. Wang and L. Yu, *et al.*, Identification of the active complex for CO oxidation over single-atom Ir-on-MgAl$_2$O$_4$ catalysts, *Nat. Catal.*, 2019, **2**(2), 149–156.

22 J. Lin, A. Wang, B. Qiao, X. Liu, X. Yang and X. Wang, *et al.*, Remarkable performance of Ir$_1$/FeO x single-atom catalyst in water gas shift reaction, *J. Am. Chem. Soc.*, 2013, **135**(41), 15314–15317.

23 M. Li, H. Wang, W. Luo, P. C. Sherrell, J. Chen and J. Yang, *et al.*, Heterogeneous single-atom catalysts for electrochemical CO$_2$ reduction reaction, *Adv. Mater.*, 2020, **32**(34), 2001848.

24 Y. Zhu, X. Yang, C. Peng, C. Priest, Y. Mei and G. Wu, Carbon-Supported Single Metal Site Catalysts for Electrochemical CO$_2$ Reduction to CO and Beyond, *Small*, 2021, **17**(16), 2005148.

25 H. Xiong, A. K. Datye and Y. Wang, Thermally Stable Single-Atom Heterogeneous Catalysts, *Adv. Mater.*, 2021, **33**(50), 2004319.

26 H. Zhang, G. Liu, L. Shi and J. Ye, Single-atom catalysts: emerging multifunctional materials in heterogeneous catalysis, *Adv. Energy Mater.*, 2018, **8**(1), 1701343.

27 H. Oschinski, Á. Morales-García and F. Illas, Interaction of First Row Transition Metals with M$_2$C (M = Ti, Zr, Hf, V, Nb, Ta, Cr, Mo, and W) MXenes: A Quest for Single-Atom Catalysts, *J. Phys. Chem. C*, 2021, **125**(4), 2477–2484.

28 M. Zhang, C. Lai, B. Li, S. Liu, D. Huang and F. Xu, *et al.*, MXenes as Superexcellent Support for Confining Single Atom: Properties, Synthesis, and Electrocatalytic Applications, *Small*, 2021, **17**(29), 2007113.

29 S. Baskaran and J. Jung, Mo$_2$CS$_2$-MXene supported single-atom catalysts for efficient and selective CO$_2$ electrochemical reduction, *Appl. Surf. Sci.*, 2022, **592**(1), 153339.

30 H. Zhou, Z. Chen and A. V. López, *et al.*, Engineering the Cu/Mo$_2$CT$_x$ (MXene) interface to drive CO$_2$ hydrogenation to methanol, *Nat. Catal.*, 2021, **4**, 860–871.

31 S. Docherty and C. Copéret, *J. Am. Chem. Soc.*, 2021, **143**(18), 6767–6780.

32 M. S. Duyar, C. Tsai, J. L. Snider, J. A. Singh, A. Gallo and J. S. Yoo, *et al.*, A Highly Active Molybdenum Phosphide Catalyst for Methanol Synthesis from CO and CO$_2$, *Angew. Chem., Int. Ed.*, 2018, **57**, 15045–15050.

33 J. Kim, B. B. Sarma, E. Andrés, N. Pfänder, P. Concepción and G. Prieto, Surface Lewis Acidity of Periphery Oxide Species as a General Kinetic Descriptor for CO$_2$ Hydrogenation to Methanol on Supported Copper Nanoparticles, *ACS Catal.*, 2019, **9**(11), 10409–10417.

34 M. Zabilskiy, V. L. Sushkevich and D. Palagin, *et al.*, The unique interplay between copper and zinc during catalytic carbon dioxide hydrogenation to methanol, *Nat. Commun.*, 2020, **11**, 2409.

35 Z. Zhang, X. Chen and J. Kang, *et al.*, The active sites of Cu–ZnO catalysts for water gas shift and CO hydrogenation reactions, *Nat. Commun.*, 2021, **12**, 4331.

36 N. D. Nielsen, J. Thrane and A. D. Jensen, *et al.*, Bifunctional Synergy in CO Hydrogenation to Methanol with Supported Cu, *Catal. Lett.*, 2020, **150**, 1427–1433.

37 A. Müller, A. Comas-Vives and C. Copéret, Ga and Zn increase the oxygen affinity of Cu-based catalysts for the CO$_x$ hydrogenation according to ab initio atomistic thermodynamics, *Chem. Sci.*, 2022, **13**, 13442–13458.

38 A. Müller, A. Comas-Vives and C. Copéret, Shape and Surface Morphology of Copper Nanoparticles under CO$_2$ Hydrogenation Conditions from First Principles, *J. Phys. Chem. C*, 2020, **125**(1), 396–409.

39 E. Lam, J. J. Corral-Pérez, K. Larmier, G. Noh, P. Wolf, A. Comas-Vives, A. Urakawa and C. Copéret, CO$_2$ Hydrogenation on Cu/Al$_2$O$_3$: Role of the Metal/Support Interface in Driving Activity and Selectivity of a Bifunctional Catalyst, *Angew. Chem., Int. Ed.*, 2019, **58**(39), 13989–13996.

40 K. Larmier, W. C. Liao, S. Tada, E. Lam, R. Verel, A. Bansode, A. Urakawa, A. Comas-Vives and C. Copéret, CO$_2$-to-Methanol Hydrogenation on Zirconia-Supported Copper Nanoparticles: Reaction Intermediates and the Role of the Metal Support Interface, *Angew. Chem., Int. Ed.*, 2017, **56**(9), 2318–2323.

41 F. Studt, M. Behrens, E. L. Kunkes, N. Thomas, S. Zander and A. Tarasov, *et al.*, The mechanism of CO and CO$_2$ hydrogenation to methanol over Cu-based catalysts, *ChemCatChem*, 2015, **7**(7), 1105–1111.

42 H. Ruland, H. Song, D. Laudenschleger, S. Stürmer, S. Schmidt and J. He, *et al.*, CO$_2$ hydrogenation with Cu/ZnO/Al$_2$O$_3$: a benchmark study, *ChemCatChem*, 2020, **12**(12), 3216–3222.

43 J. Nakamura, Y. Choi and T. Fujitani, On the Issue of the Active Site and the Role of ZnO in Cu/ZnO Methanol Synthesis Catalysts, *Top. Catal.*, 2003, **22**, 277–285.

This journal is © The Royal Society of Chemistry 2024

Catal. Sci. Technol., 2024, **14**, 6904–6916 | **6915**

44 G. Wang, S. Mine and D. Chen, *et al.*, Accelerated discovery of multi-elemental reverse water-gas shift catalysts using extrapolative machine learning approach, *Nat. Commun.*, 2023, **14**, 5861.

45 C. Zhou, J. Zhang, Y. Fu and H. Dai, Recent Advances in the RWG Conversion Reaction, *Molecules*, 2023, **28**, 7657.

46 M. González-Castaño, B. Dorneanu and H. Arellano-García, *et al.*, The reverse water gas shift reaction: a process systems engineering perspective, *React. Chem. Eng.*, 2021, **6**, 954–976.

47 M. B. Fichtl, D. Schlereth, N. Jacobsen, I. Kasatkin, J. Schumann and M. Behrens, *et al.*, Kinetics of deactivation on Cu/ZnO/Al$_2$O$_3$ methanol synthesis catalysts, *Appl. Catal., A*, 2015, **502**(5), 262–270.

48 L. Grajciar, C. J. Heard, A. A. Bondarenko, M. V. Polynski, J. Meeprasert, E. A. Pidko and P. Nachtigall, Towards operando computational modeling in heterogeneous catalysis, *Chem. Soc. Rev.*, 2018, **47**, 8307–8348.

49 M. Figueras, R. A. Gutiérrez, F. Viñes, P. J. Ramírez, J. A. Rodríguez and F. Illas, Supported Molybdenum Carbide Nanoparticles as an Excellent Catalyst for CO$_2$ Hydrogenation, *ACS Catal.*, 2021, **11**(15), 9679–9687.

50 A. Jurado, Á. Morales-García, F. Viñes and F. Illas, Identifying the Atomic Layer Stacking of Mo$_2$C MXene by Probe Molecule Adsorption, *J. Phys. Chem. C*, 2021, **125**(48), 26808–26813.

51 G. Kresse and J. Hafner, Ab initio molecular dynamics for liquid metals, *Phys. Rev. B: Condens. Matter Mater. Phys.*, 1993, **47**, 558–561.

52 G. Kresse and J. Hafner, Ab initio molecular-dynamics simulation of the liquid-metal-amorphous-semiconductor transition in germanium, *Phys. Rev. B: Condens. Matter Mater. Phys.*, 1994, **49**(20), 14251–14269.

53 G. Kresse and J. Furthmüller, Efficiency of ab-initio total energy calculations for metals and semiconductors using a plane-wave basis set, *Comput. Mater. Sci.*, 1996, **6**(1), 15–50.

54 P. E. Blöchl, Projector augmented-wave method, *Phys. Rev. B: Condens. Matter Mater. Phys.*, 1994, **50**(24), 17953–17979.

55 G. Kresse and D. Joubert, From ultrasoft pseudopotentials to the projector augmented-wave method, *Phys. Rev. B: Condens. Matter Mater. Phys.*, 1999, **59**(3), 1758–1775.

56 G. Kresse and J. Hafner, Norm-conserving and ultrasoft pseudopotentials for first row and transition elements, *J. Phys.: Condens. Matter*, 1994, **6**, 8245–8257.

57 J. Wellendorff, K. T. Lundgaard, A. Møgelhøj, V. Petzold, D. D. Landis and J. K. Nørskov, *et al.*, Density functionals for surface science: exchange-correlation model development with Bayesian error estimation, *Phys. Rev. B: Condens. Matter Mater. Phys.*, 2012, **85**(23), 235149.

58 A. H. Larsen, J. J. Mortensen, J. Blomqvist, I. E. Castelli, R. Christensen and M. Dułak, *et al.*, The atomic simulation environment—a Python library for working with atoms, *J. Phys.: Condens. Matter*, 2017, **29**(27), 273002.

59 H. Jonsson, G. Mills and K. Jacobsen, *Classical and Quantum Dynamics in Condensed Phase Simulations*, ed. B. J. Berne, Singapore World Scientific, 1998, pp. 385–404.

60 W. Tang, E. Sanville and G. Henkelman, A grid-based Bader analysis algorithm without lattice bias, *J. Phys.: Condens. Matter*, 2009, **21**(8), 084204.

61 E. Sanville, S. D. Kenny, R. Smith and G. Henkelman, Improved grid-based algorithm for Bader charge allocation, *J. Comput. Chem.*, 2007, **28**(5), 899–908.

62 G. Henkelman, A. Arnaldsson and H. Jónsson, A fast and robust algorithm for Bader decomposition of charge density, *Comput. Mater. Sci.*, 2006, **36**(3), 354–360.

63 M. Yu and D. R. Trinkle, Accurate and efficient algorithm for Bader charge integration, *J. Chem. Phys.*, 2011, **134**, 064111.

64 A. Álvarez, M. Borges, J. J. Corral-Pérez, J. Giner Olcina, L. Hu, D. Cornu, R. Huang, D. Stoian and A. Urakawa, CO$_2$ Activation over Catalytic Surfaces, *ChemPhysChem*, 2017, **18**(22), 3135–3141.

6916 | *Catal. Sci. Technol.*, 2024, **14**, 6904–6916

This journal is © The Royal Society of Chemistry 2024